

# Control-Bounded ADC

Fredrik Feyling

December 2020

# List of Symbols

## Matrices and Vectors

$a$	a scalar value
$\mathbf{a}$	a column vector $(a_1 \cdots a_N)^\top \in \mathbb{R}^N$
$\mathbf{A}$	a matrix $\begin{pmatrix} a_{11} & \cdots & a_{1N} \\ \vdots & \ddots & \vdots \\ a_{M1} & \cdots & a_{MN} \end{pmatrix} \in \mathbb{R}^{M \times N}$
$\mathbf{0}_N$	an all-zero column vector of length $N$
$\mathbf{0}_{M \times N}$	an $M$ -by- $N$ all-zero matrix
$\mathbf{1}_N$	a column vector of length $N$ with all elements 1
$\mathbf{1}_{M \times N}$	an $M$ -by- $N$ matrix with all elements 1
$\mathbf{I}_N$	an $N$ -by- $N$ matrix with ones on the main diagonal and all other elements zero
$\mathbf{H}_2$	second order Hadamard matrix $\begin{pmatrix} 1 & 1 \\ 1 & -1 \end{pmatrix}$
$\mathbf{H}_N$	Hadamard matrix of order $N$ defined by $\mathbf{H}_2 \otimes \mathbf{H}_{N/2}$
$\mathbf{H}'_N$	modified Hadamard matrix $\begin{bmatrix} \mathbf{H}_{N/2} & \mathbf{0}_{N/2 \times N/2} \\ \mathbf{0}_{N/2 \times N/2} & \mathbf{H}_{N/2} \end{bmatrix}$
$\otimes$	Kronecker product
$()^\top$	transpose
$ a $	absolute value
$\ \mathbf{b}\ _p$	p-norm $(\sum_i  b_i ^p)^{1/p}$
$\ \mathbf{c}\ _\infty$	max norm, equivalent to $\max( c_1 ,  c_2 , \dots,  c_N )$

## Sets

$\mathbb{R}$	the real numbers
--------------	------------------

## Miscellaneous

$\dot{\mathbf{x}}$	elementwise time derivative $\frac{d}{dt}\mathbf{x}(t)$
--------------------	---

## Control-Bounded Conversion

$L$	input signal dimension
$N_\ell$	system order corresponding to each input channel
$N$	total system order $LN_\ell$
$\beta$	integrator gain
$\mathbf{A}$	system matrix
$\mathbf{B}$	input matrix
$\mathbf{C}$	signal observation (output) matrix
$\mathbf{\Gamma}$	control input matrix
$\tilde{\mathbf{\Gamma}}$	control observation matrix
$\mathbf{u}(t)$	input signal
$\mathbf{u}[k]$	input samples
$\hat{\mathbf{u}}[k]$	estimated input samples
$\mathbf{x}(t)$	state vector
$\mathbf{s}[k]$	control signal
$\mathbf{s}(t)$	control contribution
$\tilde{\mathbf{s}}(t)$	control observation
$\mathbf{y}(t)$	signal observation
$\check{\mathbf{y}}(t)$	fictional signal observation
$\mathbf{G}(\omega)$	analog transfer function (ATF) matrix
$\mathbf{H}(\omega)$	noise transfer function (NTF) matrix
$\mathbf{G}(\omega)\mathbf{H}(\omega)$	signal transfer function (STF) matrix

## Acronyms

AS	analog system
ATF	analog transfer function
DC	digital control
DE	digital estimator
NTF	noise transfer function
STF	signal transfer function

## Chapter 1

# Introduction

## Chapter 2

# Conventional A/D Conversion

In order to highlight how a control-bounded converter distinguishes from conventional A/D converters, some fundamentals of conventional A/D conversion is given in this chapter. A black box illustration of a general ADC is given in figure 2.1.  $u(t)$  represents the analog input and  $\hat{u}[k]$  is the digital

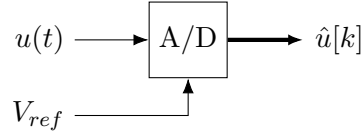


Figure 2.1: A black box representation of a general A/D converter.

output signal. For each  $k$ ,  $\hat{u}[k]$  is an  $N$ -bit digital word given by

$$\hat{u}[k] = b_1 2^{-1} + b_2 2^{-2} + \dots + b_N 2^{-N} \quad (2.1)$$

where each bit  $b_i \in \{0, 1\}$ . Assuming that the ADC produces digital outputs with a period of  $T$ , for any time instance  $t_0$ , we let  $\hat{u}[k_0]$  be the digital estimate of the continuous time input  $u(k_0 T)$ .

In figure 2.1,  $V_{ref}$  is the reference voltage used for quantization of the input. The relation between the quantities is given by

$$V_{ref} (b_1 2^{-1} + b_2 2^{-2} + \dots + b_N 2^{-N}) = u(t) \pm V_x \quad (2.2)$$

where

$$-\frac{1}{2} V_{LSB} \leq V_x < \frac{1}{2} V_{LSB} \quad (2.3)$$

and

$$V_{LSB} = \frac{V_{ref}}{2^N}. \quad (2.4)$$

$V_X$  is referred to as the quantization error, which for an ideal N-bit ADC is bounded as in (2.3). This quantization error is giving rise to the quantization noise observed in the digital output.

Conventional A/D converters can generally be divided into two main categories; Nyquist rate- and oversampling converters. These two types of A/D converters will be described briefly in the following sections.

## 2.1 Nyquist Rate A/D converters

As the name indicates, a Nyquist rate converter is related to the Nyquist sampling frequency. However, because sampling at the Nyquist rate would require a very precise anti-aliasing filter, practical converters are in general operating at a somewhat higher frequency. Following [1], a Nyquist rate A/D converter can be defined as a converter where each output value has a one-to-one correspondence with a single input value. A typical block diagram of a Nyquist rate ADC is shown in figure 2.2.

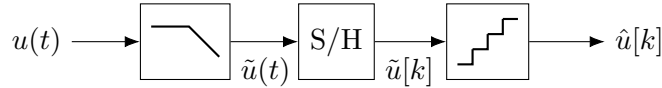


Figure 2.2: A typical Nyquist rate ADC.

In figure 2.2, the analog input  $u(t)$  is first passed through an anti-aliasing filter to suppress the higher frequency components. The signal is then sampled and held by the box labeled S/H. The sampled signal is then quantized with N-bit resolution to produce the digital output  $\hat{u}[k]$ .

## 2.2 Oversampling converters

In contrast to the Nyquist rate converter, an oversampling ADC samples the input signal at a frequency much higher than the Nyquist frequency. For an analog input signal that is bandlimited to  $f_0$ , we define the oversampling ratio as

$$\text{OSR} \triangleq \frac{f_s}{2f_0} \quad (2.5)$$

where  $f_s$  is the sampling frequency of the ADC. Sampling at a higher frequency generates redundant information about the input signal, and a single estimate of the input signal at a certain time instance is obtained by averaging several consecutive samples. The redundancy is this way utilized to give a higher resolution, or equivalently reduced requirements on the involved circuit components.

Straight forward noise shaping will itself give an improved signal-to-noise ratio (SNR) of 3dB per doubling of OSR [1]. The performance of the over-

sampling converter is further improved by noise shaping of the quantization noise, through a feedback loop with a loop filter. Such a system is known as a  $\Sigma\Delta$  ADC and the part of the system that performs the noise shaping is called a  $\Sigma\Delta$  modulator. Such a system is illustrated in figure 2.3.

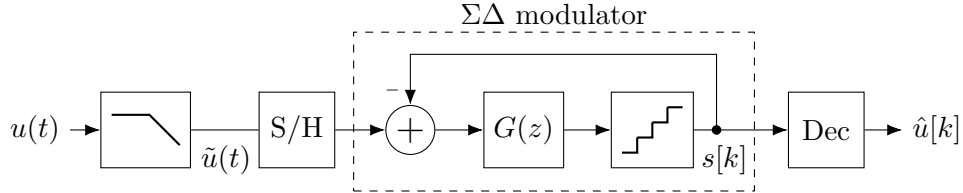


Figure 2.3: A discrete-time  $\Sigma\Delta$  ADC.

The system shown in figure 2.3 is called a discrete-time  $\Sigma\Delta$  ADC because the  $\Sigma\Delta$  modulator has a discrete-time input. A continuous time  $\Sigma\Delta$  converter is achieved by including the sampling in the feedback loop, as shown in figure 2.4. In this case, the anti-aliasing filter is part of loop filter  $G(\omega)$ .

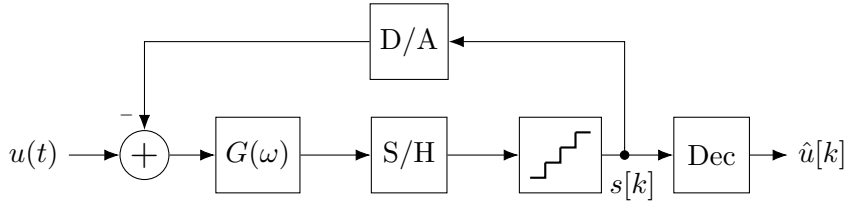


Figure 2.4: A continuous-time  $\Sigma\Delta$  ADC.

### 2.2.1 Transfer Function Analysis

The transfer function analysis of the continuous-time  $\Sigma\Delta$  modulator involves a mixture of continuous- and discrete time signals, as the transition between these domains happens inside the modulator. The analysis is straight forward, but the resulting expression is somewhat dirty. To give a clear and intuitive understanding of the transfer functions, we avoid the distinction between continuous and discrete time in this analysis. The resulting simplified system is shown in figure 2.5. The quantizer is replaced by its linear model, which approximates the quantization error as an independent signal that enters the system in an additive way.

Let  $U$ ,  $E$  and  $S$  be the signals  $u(t)$ ,  $e[k]$  and  $s[k]$  in frequency domain, where the distinction between periodic and continuous frequency domain is implicit. The output of the modulator can be expressed as

$$S = E + G[U - S] \quad (2.6)$$

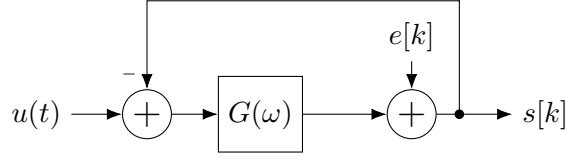


Figure 2.5: A simplified, linear model of the continuous-time  $\Sigma\Delta$  ADC.

and hence

$$S = \underbrace{\frac{1}{1+G}}_{\text{NTF}} E + \underbrace{\frac{G}{1+G}}_{\text{STF}} U. \quad (2.7)$$

From (2.7) we recognize the noise transfer function as  $\text{NTF} = \frac{1}{1+G}$  and the signal transfer function as  $\text{STF} = \frac{G}{1+G}$ . Because the input signal and the quantization noise experience different transfer functions, it is possible to shape the noise such that most of the quantization noise appears outside the frequency band of interest, while simultaneously leaving the actual signal unchanged. This is the effect known as noise shaping.



## Chapter 3

# Control-Bounded ADC

### 3.1 History and Background

Control-bounded A/D conversion is a conceptually new approach to the problem of creating a digital representation of an analog signal. The conversion technique has developed quite recently over the last years, and the progress is mainly pushed forward by prof. Hans-Andrea Loeliger et al., from the Signal and Information Processing Laboratory (ISI), ETH Zürich. The concept was first introduced at the IEEE Information Theory & Applications Workshop (ITA), february 2011 [2]. In this paper, the main building blocks of a control-bounded ADC was presented, but no explicit example of such an ADC was given, and no behavioural analysis presented. The approach was further developed in [3], which was published for the same conference in 2015. In this paper, the conversion algorithm is improved and a limited transfer function analysis is presented. The latest publication on control-bounded conversion is from 2020 [4]. This is a longer paper with the goal of providing the sufficient information for analog designers to experiment with control-bounded ADCs. The paper provides a more details on the implementation and operation of the building blocks, together with a full transfer function analysis. Measurements on a proof-of-concept hardware prototype is also presented.

In addition to the mentioned papers, Hampus Malmberg, co-author of the latest paper [4], has recently defended his Ph.D. on Control-Bounded Converters. The author of this paper has been given early access to a draft of the thesis that is not yet published [5], and this draft serves as the main source of information on this topic.

In this section, the operating principle of a control-bounded converter is described in detail, and we follow the notation established in [4]. The theoretical presentation given in this section will be very close to that of [5], but less general and limited to what is necessary for understanding the presented results.

### 3.2 Overview

The control-bounded ADC approaches the A/D conversion problem differently compared to conventional converters from section 2. The conceptual difference lies in the view on sampling. In a control-bounded converter, the analog input signal is never sampled in the conventional way. The circuit that constitutes a control-bounded ADC still contains quantizers, but the “quantized” signals are never treated as a sampled version of the input. Instead, they are intermediate digital signals that only indirectly relates to the input, and they are used by a digital estimation filter to perform the digital estimate of the input signal. This way, rather than the process of performing accurate measurements of an analog signal using imperfect circuit components, sampling becomes the process of converting a redundant digital representation into an efficient one [5].

To clarify this, consider the general block diagram shown in figure 3.1.

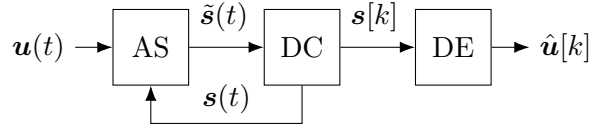


Figure 3.1: A block diagram of the control-bounded ADC

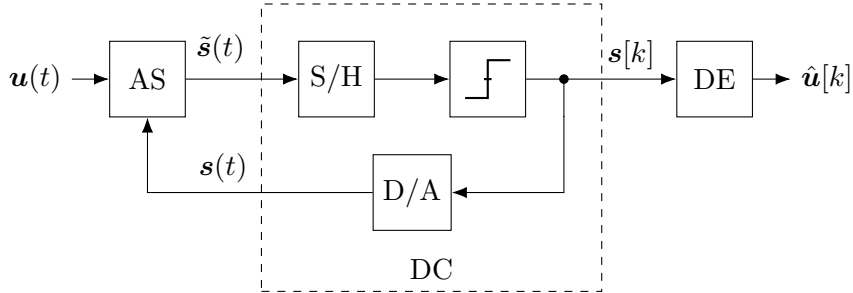


Figure 3.2: A control-bounded ADC with the DC block opened

As the figure indicates, the control-bounded ADC consists of three main building blocks; an analog system (AS), a digital control (DC) and a digital estimator (DE). The signals  $\mathbf{u}(t)$ ,  $\hat{\mathbf{u}}[k]$ ,  $\tilde{\mathbf{s}}(t)$ ,  $\mathbf{s}[k]$  and  $\mathbf{s}(t)$  are in general vector-valued functions. The analog system amplifies the input signal  $\mathbf{u}(t)$ , preferably with very high gain within the frequency band of interest. The digital control stabilizes the analog system by forcing the internal states of the system to stay within its bounds. The internal states are observed through the *control observation*  $\tilde{\mathbf{s}}(t)$  and controlled through the *control contribution*  $\mathbf{s}(t)$ . The digital estimator takes the *control signal*  $\mathbf{s}[k]$  as an input and forms the digital estimate  $\hat{\mathbf{u}}[k]$  of  $\mathbf{u}(t)$ .

Before going into detail on each of these building blocks, consider figure 3.2, which shows the same block diagram, but with the DC block opened. From this figure it is evident that the structure of the control-bounded ADC is very similar to that of the continuous-time  $\Sigma\Delta$  modulator in figure 2.4. As mentioned, the main difference between these architectures arises from the different interpretation of the control signal  $\mathbf{s}[k]$ . In the continuous-time  $\Sigma\Delta$ , this signal is viewed as a sampled and quantized version of the input signal and the digital output is obtained by averaging this signal through a decimation filter. In the control-bounded perspective the direct relation between  $\mathbf{s}[k]$  and  $\mathbf{u}(t)$  is ignored completely. Instead, we focus solely on the fact that  $\mathbf{s}(t)$  is contribution needed to stabilize the internal states of the analog system. This view leads to a different estimation filter for the reconstruction of  $\hat{\mathbf{u}}[k]$ .

It should be noted that the contribution of the control-bounded ADC is not to provide an alternative decimation filter to already existing  $\Sigma\Delta$  ADCs. As shown in section 2.2.1, the noise shaping of the  $\Sigma\Delta$  modulator relies on the fact that the signal and the quantization noise enters the system at different points in the signal flow. This condition is a major restriction to the design space of  $\Sigma\Delta$  modulators. The estimation filter of the control-bounded converter on the other hand, imposes no restrictions to the analog system. Hence, the ADC can be designed with combinations of analog system and digital control that have previously been unimaginable. The advantage of this will become more apparent when we consider the Hadamard ADC in chapter 5.

### 3.3 Analog System

The analog system, here assumed to be a continuous time filter, sets the frequency response of the overall ADC, and is designed to amplify the frequency band of interest. As stability of the analog system is controlled digitally, the analog system itself need not be stable.

#### 3.3.1 State Space Model

The dynamics of the analog system is described using a state space model notation, illustrated in figure 3.3. The multi-channel input signal  $\mathbf{u}(t)$ , the state-vector  $\mathbf{x}(t)$  and the control contribution  $\mathbf{s}(t)$  is related by the differential equation

$$\dot{\mathbf{x}}(t) = \mathbf{A}\mathbf{x}(t) + \mathbf{B}\mathbf{u}(t) + \mathbf{\Gamma}\mathbf{s}(t). \quad (3.1)$$

where

$$\mathbf{u}(t) \triangleq (u_1(t), \dots, u_L(t))^T \in \mathbb{R}^L, \quad (3.2)$$

$$\mathbf{x}(t) \triangleq (x_1(t), \dots, x_N(t))^T \in \mathbb{R}^N \quad (3.3)$$

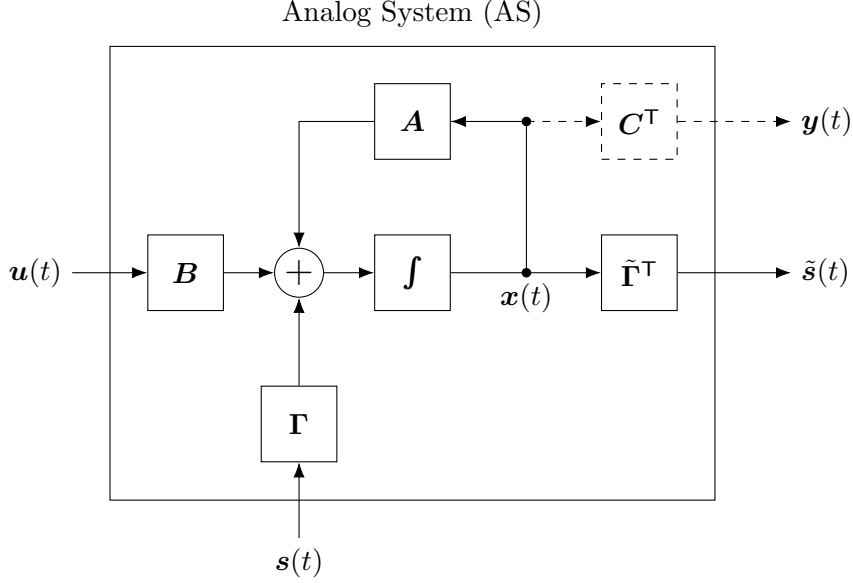


Figure 3.3: State space model of the AS.

and

$$\mathbf{s}(t) \triangleq (s_1(t), \dots, s_M(t))^T \in \mathbb{R}^M. \quad (3.4)$$

This system is said to have  $L$  inputs,  $M$  controls and  $N$  states. We will refer to  $\mathbf{A} \in \mathbb{R}^{N \times N}$ ,  $\mathbf{B} \in \mathbb{R}^{N \times L}$  and  $\mathbf{\Gamma} \in \mathbb{R}^{N \times M}$  as the *system matrix*, the *input matrix* and the *control input matrix* respectively.

The only physical output of the analog system is the control observation

$$\tilde{\mathbf{s}}(t) \triangleq \tilde{\mathbf{\Gamma}}^T \mathbf{x}(t) \in \mathbb{R}^{\tilde{M}}, \quad (3.5)$$

which is used by the digital control to produce the control signal  $\mathbf{s}[k]$ . The control observation is a linear mapping of the internal state-vector, through the *control observation matrix*  $\tilde{\mathbf{\Gamma}}^T \in \mathbb{R}^{\tilde{M} \times N}$ . The second output of the analog system is the purely conceptual signal

$$\mathbf{y}(t) \triangleq \mathbf{C}^T \mathbf{x}(t) \in \mathbb{R}^{\tilde{N}}, \quad (3.6)$$

which is used by the digital estimator to produce the estimate  $\hat{\mathbf{u}}[k]$ . This signal has no physical meaning, and the *signal observation matrix*  $\mathbf{C}^T \in \mathbb{R}^{\tilde{N} \times N}$  is basically telling the digital estimation algorithm which of the internal states that could be treated as bounded. Thus  $\mathbf{y}(t)$  and  $\mathbf{C}^T$  does only exist numerically inside the digital estimator.

### 3.3.2 Transfer Function and Impulse Response Matrix

The transfer function of the analog system gives the frequency domain relation between the input  $\mathbf{U}(\omega)$  and the output  $\mathbf{Y}(\omega)$ . Hence for the general

case of  $L$  inputs and  $\tilde{N}$  outputs, the analog transfer function (ATF) is a  $\tilde{N}$ -by- $L$  matrix, defined by  $\mathbf{Y}(\omega) = \mathbf{G}(\omega)\mathbf{U}(\omega)$ . Each element  $G_{i,j}(\omega)$  of  $\mathbf{G}(\omega)$  is the transfer function from  $U_j(\omega)$  to  $Y_i(\omega)$ . From (3.1) the frequency domain relation between the input and the state vector is obtained as

$$j\omega\mathbf{X}(\omega) = \mathbf{A}\mathbf{X}(\omega) + \mathbf{B}\mathbf{U}(\omega) \quad (3.7)$$

$$(j\omega\mathbf{I}_N - \mathbf{A})\mathbf{X}(\omega) = \mathbf{B}\mathbf{U}(\omega) \quad (3.8)$$

$$\mathbf{X}(\omega) = (j\omega\mathbf{I}_N - \mathbf{A})^{-1} \mathbf{B}\mathbf{U}(\omega). \quad (3.9)$$

The output vector is obtained by multiplying the state vector with the signal observation matrix,  $\mathbf{C}^\top$ . Hence

$$\mathbf{Y}(j\omega) = \mathbf{C}^\top (j\omega\mathbf{I}_N - \mathbf{A})^{-1} \mathbf{B}\mathbf{U}(j\omega) \quad (3.10)$$

and we recognize the ATF as

$$\mathbf{G}(\omega) = \mathbf{C}^\top (j\omega\mathbf{I}_N - \mathbf{A})^{-1} \mathbf{B}. \quad (3.11)$$

The analog impulse response matrix is then obtained from the inverse Laplace transform as

$$\mathbf{g}(t) = \mathbf{C}^\top \exp(\mathbf{A}t)\mathbf{B}, \quad (3.12)$$

where  $\exp$  denotes the matrix exponential.

### 3.4 Digital Control

The digital control is a discrete time system which serves the purpose of stabilizing the analog system. It includes a sample-and-hold circuit, a one-bit quantizer and a D/A converter, as shown in figure 3.2. The control observation  $\tilde{\mathbf{s}}(t)$  is sampled and quantized with a sampling period  $T$ , resulting in the digital control signal  $\mathbf{s}[k]$  which is passed on to the digital estimator. The D/A converter is a non-return to zero (NRZ) DAC generating the control contribution  $\mathbf{s}(t)$ .

The digital control is called effective if it manages to keep the state vector bounded, given a bounded input vector. The input vector  $\mathbf{u}(t)$  is bounded if it satisfies

$$\|\mathbf{u}(t)\|_\infty \leq b_{\mathbf{u}} \quad \forall t. \quad (3.13)$$

Equivalently, the state vector  $\mathbf{x}(t)$  is bounded if it satisfies

$$\|\mathbf{x}(t)\|_\infty \leq b_{\mathbf{x}} \quad \forall t. \quad (3.14)$$

In this paper, the input signal will always be assumed bounded, and the boundary  $b_{\mathbf{u}}$  is assumed to be set by an external circuit. The boundary for the state vector,  $b_{\mathbf{x}}$ , is a free variable and determines the magnitude of the state vector of the analog system.

A thorough analysis of the criteria for an effective control is found in [5]. The analysis is useful for the theoretical understanding of the system, but not necessary for the design process and is therefore beyond the scope of this paper. Intuitively, there are three quantities affecting the stability of the analog system. The sampling period  $T$  of the digital control, the unity gain frequency of the analog system and the boundary  $b_{\mathbf{x}}$ . Increasing the speed of the analog system would require a shorter sampling period to counteract the faster growth of the system states. Reducing the boundary  $b_{\mathbf{x}}$  would require either reducing the speed of the analog system or increasing the sampling frequency, in order to maintain a tighter bound.

It will become apparent in the next section that the performance of the overall ADC is related to the digital controls ability to bound the state vector. Designing the ADC for a stability guarantee means that it is theoretically impossible for the state vector to grow beyond  $b_{\mathbf{x}}$  at any point in time, given any valid input signal. This will of course result in a very large stability margin most of the time, which means that there is potential for increased performance not being utilized. The preferred way of tuning the stability of the system is therefore through simulations, and then to include the possibility of a full system reset if it happens to become unstable.

### 3.5 Digital Estimator

The digital estimator (DE) forms an estimate  $\hat{\mathbf{u}}[k]$  of  $\mathbf{u}(t)$  based on the control signals  $\mathbf{s}[k]$  and the knowledge of the AS system parameters. The purpose of this section is to describe the digital estimation problem, and to derive the optimum linear estimation filter. The resulting estimate of  $\mathbf{u}(t)$  is a continuous time estimate  $\hat{\mathbf{u}}(t)$  that can be computed at an arbitrary time instance. In the derivation of the estimation filter, the estimate is therefore denoted by  $\hat{\mathbf{u}}(t)$  instead of  $\hat{\mathbf{u}}[k]$ .

#### 3.5.1 Statistical Estimation Problem and Transfer Functions

In the following analysis, the system described by (3.1) is assumed to be invariant and stable. This assumption only applies in the analysis of this section, where the goal is to describe the estimation problem and derive the analytic transfer function expressions. The actual estimation filter will not be limited by these assumptions.

The objective of the digital estimator is to construct a digital estimate  $\hat{\mathbf{u}}(t)$  of  $\mathbf{u}(t)$ , based on the control signals  $\mathbf{s}[k]$ . As highlighted previously in this chapter, the direct relation between  $\mathbf{s}[k]$  and  $\mathbf{u}(t)$  is ignored completely by the digital estimator. Instead,  $\mathbf{s}[k]$  is only treated as the signal needed to stabilize the analog system, when triggered by an input signal  $\mathbf{u}(t)$ .

To formalize this approach, let  $\tilde{\mathbf{y}}(t) \triangleq (\mathbf{g} * \mathbf{u})(t) \in \mathbb{R}^{\tilde{N}}$  be the signal that would have occurred at the output of the analog system in the absence of

any digital control. Furthermore, let  $\mathbf{q}(t)$  be the control contribution signal seen at the output of the analog system. Because the control contribution enters the analog system in an additive way, we can express the relation as

$$\mathbf{y}(t) = \check{\mathbf{y}}(t) - \mathbf{q}(t). \quad (3.15)$$

The situation is illustrated in figure 3.4. In this figure, solid lines represent the physical components of the ADC, while dashed lines represents conceptual quantities that only exist inside the digital estimator. It is illustrated how  $\mathbf{q}(t)$  relates to the control contribution  $\mathbf{s}(t)$ . Because the digital estimator knows the parametrization of the analog system, as well as the waveform of the D/A converter,  $\mathbf{q}(t)$  is (in principle) known from the observation of  $\mathbf{s}[k]$ . Note that this illustration is only meant to illustrate the estimation problem of the digital estimator, not to show how the actual estimate is computed. We denote the frequency response of the digital estimation filter by  $\mathbf{H}(\omega)$  and the continuous time estimate  $\hat{\mathbf{u}}(t)$  of  $\mathbf{u}(t)$  is obtained by

$$\hat{\mathbf{u}}(t) = (\mathbf{h} * \mathbf{q})(t) \in \mathbb{R}^L. \quad (3.16)$$

Because the objective of the analog system is to greatly amplify the sought frequency content of  $\mathbf{u}(t)$ , both  $\|\check{\mathbf{y}}(t)\|_\infty$  and  $\|\mathbf{q}(t)\|_\infty$  will be very large compared to  $\|\mathbf{y}(t)\|_\infty$ , which is bounded due to (3.14). We can therefore approximate  $\check{\mathbf{y}}(t) \approx \mathbf{q}(t)$  which is equivalent to the approximation  $\mathbf{y}(t) \approx \mathbf{0}$ . Hence we write the estimate as

$$\hat{\mathbf{u}}(t) = (\mathbf{h} * \mathbf{q})(t) \quad (3.17)$$

$$= (\mathbf{h} * \check{\mathbf{y}})(t) - (\mathbf{h} * \mathbf{y})(t) \quad (3.18)$$

$$= (\mathbf{h} * \mathbf{g} * \mathbf{u})(t) - (\mathbf{h} * \mathbf{y})(t) \quad (3.19)$$

$$\approx (\mathbf{h} * \mathbf{g} * \mathbf{u})(t) \quad (3.20)$$

From (3.19) it is evident that  $\hat{\mathbf{u}}(t)$  could have been computed with arbitrary accuracy, if the output  $\mathbf{y}(t)$  was known to the digital estimator. This if statement is obvious, but it illustrates an important point. Instead of relying on an inevitably inaccurate measurement of  $\mathbf{y}(t)$ , we approximate this signal as constantly being zero. The accuracy of the estimate then relies on the validity of the approximation  $\mathbf{y}(t) \approx \mathbf{0}$ , rather than the precision of a direct measurement of  $\mathbf{y}(t)$ . Any deviation of  $\mathbf{y}(t)$  from  $\mathbf{0}$  will result in a conversion error, meaning that  $\mathbf{y}(t)$  is the conversion error signal seen at the output of the analog system. This conversion error does not enter the estimate directly, but is filtered by  $\mathbf{h}(t)$ . From the Fourier transform of (3.19),

$$\hat{\mathbf{U}}(\omega) = \underbrace{\mathbf{H}(\omega)\mathbf{G}(\omega)}_{\text{STF}}\mathbf{U}(\omega) - \underbrace{\mathbf{H}(\omega)}_{\text{NTF}}\mathbf{Y}(\omega), \quad (3.21)$$

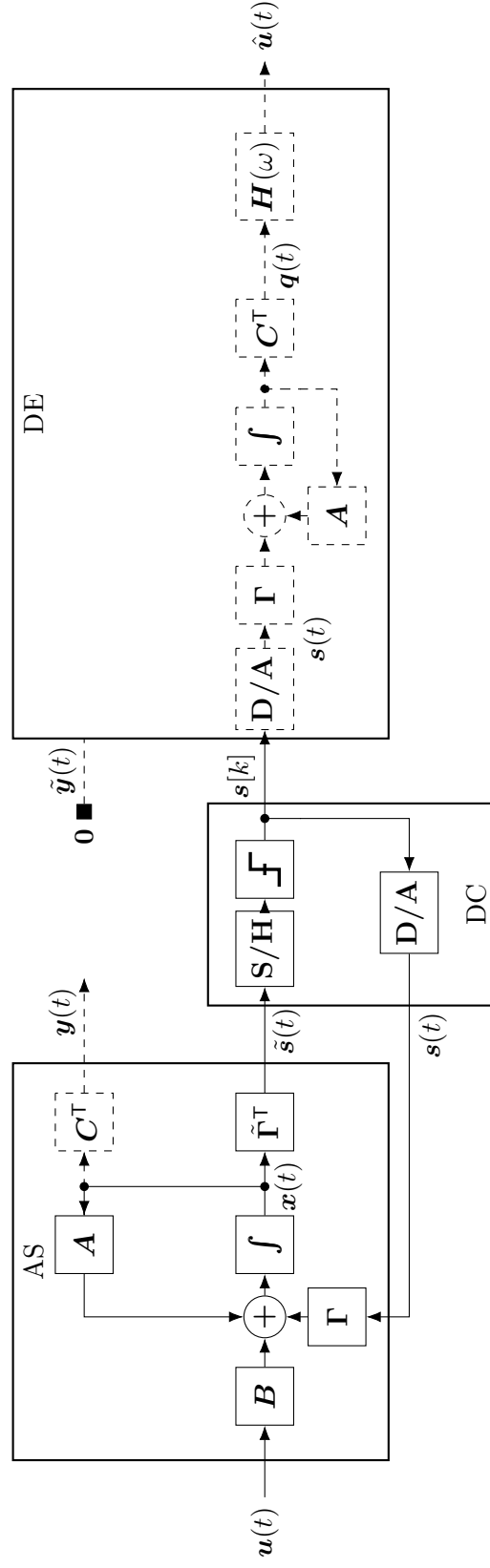


Figure 3.4: Block diagram of the complete control-bounded ADC, with the digital estimation problem visualized. The approximation  $y(t) \approx \tilde{y}(t) = \mathbf{0}$  is indicated by the fixed observation of  $\tilde{y}(t) = \mathbf{0}$  outside the DE box.



we recognize the noise and signal transfer functions as  $\text{STF} = \mathbf{H}(\omega)\mathbf{G}(\omega)$  and  $\text{NTF} = \mathbf{H}(\omega)$  respectively.

The derivation of the estimation filter is carried out in detail in [5] and only the main results is presented in this paper. In the derivation, both  $\mathbf{y}(t)$  and  $\mathbf{u}(t)$  is assumed to be independent, centered, multivariate and wide-sense stationary stochastic processes. The estimation filter is then determined by

$$\mathbf{h}(t) = \underset{\bar{\mathbf{h}}}{\operatorname{argmin}} \mathbb{E}[(\hat{\mathbf{u}}(t) - \mathbf{u}(t))^2] \quad (3.22)$$

$$= \underset{\bar{\mathbf{h}}}{\operatorname{argmin}} \mathbb{E}[(\bar{\mathbf{h}} * \mathbf{q})(t) - \mathbf{u}(t)]^2. \quad (3.23)$$

This minimization problem is exactly the objective of the Wiener-filter [6], and the impulse response matrix is given by the solution to the well known Wiener-Hopf equations:

$$(\mathbf{h} * \mathbf{R}_{\mathbf{q}\mathbf{q}^\top})(\tau) = \mathbf{R}_{\mathbf{u}\mathbf{q}^\top}(-\tau) \quad (3.24)$$

where

$$\mathbf{R}_{\mathbf{q}\mathbf{q}^\top} \triangleq \mathbb{E}[\mathbf{q}(t)\mathbf{q}(t+\tau)^\top] \quad (3.25)$$

$$\mathbf{R}_{\mathbf{u}\mathbf{q}^\top} \triangleq \mathbb{E}[\mathbf{u}(t)\mathbf{q}(t+\tau)^\top] \quad (3.26)$$

are the autocovariance and cross-covariance matrices respectively. By taking the Fourier transform of (3.24) we obtain the frequency response matrix  $\mathbf{H}(\omega)$  as

$$\mathbf{H}(\omega) = \mathbf{G}^\text{H}(\omega) \left( \mathbf{G}(\omega)\mathbf{G}^\text{H}(\omega) + \eta^2 \mathbf{I}_N \right)^{-1}, \quad (3.27)$$

and the reader is referred to [5] for computational details. The parameter  $\eta$  is defined as

$$\eta \triangleq \frac{\sigma_{\mathbf{y}}^2}{\sigma_{\mathbf{u}}^2}, \quad (3.28)$$

where  $\sigma_{\mathbf{y}}^2$  and  $\sigma_{\mathbf{u}}^2$  are the power spectral densities of  $\mathbf{y}(t)$  and  $\mathbf{u}(t)$  respectively.

### 3.5.2 Estimation filter implementation

With the digital estimation filter described by (3.27), the estimation could in principle be carried out by computing  $\hat{\mathbf{u}}(t)$  as in (3.16). This computation is however not straight forward. First of all, the elements of  $\mathbf{q}(t)$  will necessarily be very large in magnitude, as this was the condition for the approximation (3.20). Carrying out a continuous time convolution with this unbounded signal would obviously lead to numerical problems. In addition the computation of  $\mathbf{q}(t)$  from  $\mathbf{s}[k]$ , as illustrated in figure 3.4 might be computationally expensive.

In [2] it was shown that the estimate  $\hat{\mathbf{u}}(t)$  can be computed in an alternative way, using a non-standard version of the Kalman smoothing algorithm. This algorithm converges to the estimate (3.16) as the considered time window extends towards infinity. The algorithm is also indifferent to the stability assumptions made in the previous section. In this section, a concise description of the filter algorithm is given, and the reader is referred to [4] for the derivation.

The algorithm consist of a forward recursion

$$\vec{\mathbf{m}}_{k+1} \triangleq \mathbf{A}_f \vec{\mathbf{m}}_k + \mathbf{B}_f \mathbf{s}[k], \quad (3.29)$$

a backward recursion

$$\overleftarrow{\mathbf{m}}_{k-1} \triangleq \mathbf{A}_b \overleftarrow{\mathbf{m}}_k + \mathbf{B}_b \mathbf{s}[k-1], \quad (3.30)$$

and finally the estimate

$$\hat{\mathbf{u}}(t_k) \triangleq \mathbf{W}^\top (\overleftarrow{\mathbf{m}}_k - \vec{\mathbf{m}}_k). \quad (3.31)$$

The matrices  $\mathbf{A}_f, \mathbf{A}_b, \mathbf{B}_f, \mathbf{B}_b$  and  $\mathbf{W}$  is computed offline, and is given by the following equations.

$$\mathbf{A}_f \triangleq \exp \left( \left( \mathbf{A} - \frac{1}{\eta^2} \vec{\mathbf{V}} \right) T \right) \quad (3.32)$$

$$\mathbf{A}_b \triangleq \exp \left( - \left( \mathbf{A} + \frac{1}{\eta^2} \overleftarrow{\mathbf{V}} \right) T \right) \quad (3.33)$$

$$\mathbf{B}_f \triangleq \int_0^T \exp \left( \left( \mathbf{A} - \frac{1}{\eta^2} \vec{\mathbf{V}} \right) (T - \tau) \right) \mathbf{\Gamma} d\tau \quad (3.34)$$

$$\mathbf{B}_b \triangleq - \int_0^T \exp \left( - \left( \mathbf{A} + \frac{1}{\eta^2} \overleftarrow{\mathbf{V}} \right) (T - \tau) \right) \mathbf{\Gamma} d\tau \quad (3.35)$$

In equations (3.32 - 3.35),  $\exp(\cdot)$  denotes the matrix exponential, which is not to be confused with the element-wise exponential operation.

The matrices  $\vec{\mathbf{V}}$  and  $\overleftarrow{\mathbf{V}}$  used in (3.32 - 3.35) is obtained by solving the continuous-time algebraic Riccati (CARE) equations

$$\mathbf{A} \vec{\mathbf{V}} + (\mathbf{A} \vec{\mathbf{V}})^\top + \mathbf{B} \mathbf{B}^\top - \frac{1}{\eta^2} \vec{\mathbf{V}} \mathbf{C}^\top \mathbf{C} \vec{\mathbf{V}} = \mathbf{0}_{N \times N} \quad (3.36)$$

and

$$\mathbf{A} \overleftarrow{\mathbf{V}} + (\mathbf{A} \overleftarrow{\mathbf{V}})^\top - \mathbf{B} \mathbf{B}^\top + \frac{1}{\eta^2} \overleftarrow{\mathbf{V}} \mathbf{C}^\top \mathbf{C} \overleftarrow{\mathbf{V}} = \mathbf{0}_{N \times N}. \quad (3.37)$$

The matrix  $\mathbf{W}$  is finally obtained by solving the linear equation system

$$(\vec{\mathbf{V}} + \overleftarrow{\mathbf{V}}) \mathbf{W} = \mathbf{B}. \quad (3.38)$$

### 3.5.3 Practical Remarks

We conclude this section with some practical considerations.

#### Controlling the Filter Bandwidth

In (3.28) the parameter  $\eta$  was defined in terms of the power spectral densities of  $\mathbf{y}(t)$  and  $\mathbf{u}(t)$ , when these signals are modeled as independent stochastic processes. In practice however,  $\eta$  is a free variable and is used by the designer to control the bandwidth of the estimation filter. To see this, consider the scalar input case where both  $\mathbf{G}(\omega)$  and  $\mathbf{H}(\omega)$  are column vectors. In this case, the noise transfer function (3.27) reduces to

$$\mathbf{H}(\omega) = \text{NTF} = \frac{\mathbf{G}^H(\omega)}{\|\mathbf{G}(\omega)\|_2^2 + \eta^2} \in \mathbb{C}^{1 \times \tilde{N}}, \quad (3.39)$$

and the signal transfer function becomes

$$\text{STF} = \frac{\|\mathbf{G}(\omega)\|_2^2}{\|\mathbf{G}(\omega)\|_2^2 + \eta^2} \in \mathbb{R}. \quad (3.40)$$

Assuming  $\|\mathbf{G}(\omega)\|_\infty$  is monotonically decreasing in  $\omega$ , the bandwidth of the digital estimator may be defined in terms of the critical frequency,  $\omega_c$ , as

$$\|\mathbf{G}(\omega_c)\|_2^2 = \eta^2. \quad (3.41)$$

#### Signal-to-Noise Ratio

An analytic derivation of the SNR of the control-bounded ADC is given in [4]. The analysis models the output of the analog system,  $\mathbf{y}(t)$ , as white noise, i.e. assuming the power spectral density is given by  $\mathbf{S}_{\mathbf{y}\mathbf{y}^\top}(\omega) \approx \sigma_{\mathbf{y}|\mathcal{B}}^2 \mathbf{I}_{\tilde{N}}$ . In this expression,  $\mathcal{B}$  denotes the frequency band of interest and  $\sigma_{\mathbf{y}|\mathcal{B}}^2$  is the variance of  $\mathbf{y}(t)$  within this frequency band. From this assumption an approximated expression for the SNR is obtained as

$$\text{SNR} \approx \frac{\sigma_{\mathbf{y}|\mathcal{B}}^2}{2\pi} \int_{\omega \in \mathcal{B}} \frac{1}{\|\mathbf{G}(\omega)\|_2^2} d\omega. \quad (3.42)$$

Even though this is an approximation it reveals a useful intuition of how the quantities that affect the performance of the ADC.  $\sigma_{\mathbf{y}|\mathcal{B}}^2$  relates to the magnitude of  $\mathbf{y}(t)$ , and is minimized by tightening the control bound  $b_{\mathbf{x}}$ . Therefore, a tight control bound together with a high analog system gain result in large SNR.

The SNR is also related to the bandwidth parameter  $\eta$ , as seen by considering the ratio between the STF and NTF

$$\frac{\text{STF}(\omega_c)}{\|\mathbf{H}(\omega_c)\|_2} = \frac{\|\mathbf{G}(\omega_c)\|_2^2}{\|\mathbf{G}(\omega_c)\|_2^2 + \eta^2} \left( \frac{\|\mathbf{G}(\omega_c)\|_2}{\|\mathbf{G}(\omega_c)\|_2^2 + \eta^2} \right)^{-1} \quad (3.43)$$

$$= \|\mathbf{G}(\omega_c)\|_2 \quad (3.44)$$

$$= \eta. \quad (3.45)$$

Therefore a trade-off has to be made between the bandwidth of the ADC and the suppression of the conversion error. This is similar to the trade-off in a  $\Sigma\Delta$  ADC when considering the cut-off frequency of the decimation filter. This trade-off will be exemplified when a particular ADC implementation is considered in the following chapters.

## Chapter 4

# The Chain-of-Integrators ADC

## Chapter 5

# Hadamard ADC

The main advantage of control-bounded ADCs is flexibility. The only requirement set on the system by the estimation filter is that it obeys the differential equations (3.1). This flexibility allows the designer to tailor the system against the application to a larger degree than what is possible in conventional ADC.

The application of this work is modern high-end ultrasound probes. Such probes have up to 10,000 transducers stacked in a 2D array, and the large number of transducers is used for beamforming. With today's technology, having 10,000 ADCs inside the probe is not possible due to restrictions on area and current consumption. Today's solutions therefore employ combinations of analog and digital beamforming, dividing the transducer array into sub arrays sharing one ADC. The transducers of each sub array are combined with analog delay-and-add techniques. Having full control of each transducer would of course be favorable.

In this work, we want to take advantage of this large number of input channels. Instead of converting each channel individually we view the problem of converting 10,000 analog signals as one big task, resulting in one huge ADC instead of 10,000 smaller ones. The goal is that the resulting ADC will have a current consumption less than 10,000 times a single state-of-the-art ADC.

The Hadamard ADC is based on the chain-of-integrator ADC and apply the Hadamard matrix,  $\mathbf{H}_N$ , to rotate the state vector of the analog system. For  $N$  being powers of two, the Hadamard matrix is defined recursively as

$$\mathbf{H}_N = \mathbf{H}_2 \otimes \mathbf{H}_{N/2} \quad (5.1)$$

where

$$\mathbf{H}_2 = \begin{pmatrix} 1 & 1 \\ 1 & -1 \end{pmatrix} \quad (5.2)$$

The Hadamard matrix is an orthogonal matrix with the useful properties

$$\mathbf{H}_N = \mathbf{H}_N^\top \quad (5.3)$$

and

$$\mathbf{H}_N^\top \mathbf{H}_N = N \mathbf{I}_N. \quad (5.4)$$

When transforming the state vector, the energy from all input channels will be equally distributed over all involved components. The consequence of this is that the overall ADC can be scaled towards the average, rather than the maximum signal energy. Depending on the spatial peak-to-average ration of the input channels, this will result in a gain of SNR, as will be further explored the next chapter.

## 5.1 Analog System

The Hadamard ADC is described by the equations

$$\dot{\mathbf{x}}(t) = \mathbf{A}\mathbf{x}(t) + \mathbf{B}\mathbf{u}(t) + \mathbf{\Gamma}\mathbf{s}(t) \quad (5.5)$$

$$\mathbf{y}(t) = \mathbf{C}^\top \mathbf{x}(t) \quad (5.6)$$

and

$$\tilde{\mathbf{s}}(t) = \tilde{\mathbf{\Gamma}}^\top \mathbf{x}(t). \quad (5.7)$$

The AS is determined solely by  $\mathbf{A}$ ,  $\mathbf{B}$  and  $\mathbf{C}^\top$ .  $\mathbf{\Gamma}$  and  $\tilde{\mathbf{\Gamma}}^\top$  only affects the performance of the DC which will be described in the next section. The state-space matrices  $\mathbf{A}$ ,  $\mathbf{B}$  and  $\mathbf{C}^\top$  must be chosen such that the desired state-vector rotation is obtained, and at the same time provide high gain within the frequency band of interest. In addition, the parametrization should allow an energy efficient hardware implementation.

The proposed system is described by

$$\mathbf{A} = \mathbf{H}'_N \mathbf{A}' \in \mathbb{R}^{N \times N}, \quad (5.8)$$

$$\mathbf{B} = \mathbf{H}'_N \mathbf{B}' \in \mathbb{R}^{N \times L} \quad (5.9)$$

and

$$\mathbf{C} = \mathbf{C}' \in \mathbb{R}^{N \times L}, \quad (5.10)$$

where

$$\mathbf{H}'_N = \begin{bmatrix} \mathbf{H}_{N/2} & \mathbf{0}_{N/2} \\ \mathbf{0}_{N/2} & \mathbf{H}_{N/2} \end{bmatrix} \in \mathbb{R}^{N \times N} \quad (5.11)$$

and

$$\mathbf{A}' = \begin{bmatrix} \mathbf{0}_{N/2} & \beta \mathbf{L}_{N/2} \\ \beta \mathbf{I}_{N/2} & \mathbf{0}_{N/2} \end{bmatrix} \in \mathbb{R}^{N \times N}. \quad (5.12)$$

The matrix  $\mathbf{A}'$  is described as a block matrix and the sub-matrix  $\mathbf{A}_{21} = \beta \mathbf{L}_{N/2}$  is a strictly lower triangular matrix. For the single input case,

$$\mathbf{L}_{N/2} = \begin{pmatrix} 0 & & & & \\ 1 & 0 & & & \\ 0 & 1 & 0 & & \\ \vdots & \ddots & \ddots & \ddots & \\ 0 & \cdots & 0 & 1 & 0 \end{pmatrix} \in \mathbb{R}^{\frac{N}{2} \times \frac{N}{2}}, \quad (5.13)$$

$$\mathbf{B}' = (1 \quad 0 \quad \cdots \quad 0)^\top \in \mathbb{R}^{N \times L} \quad (5.14)$$

and

$$\mathbf{C}' = (0 \quad 0 \quad \cdots \quad 1)^\top \in \mathbb{R}^{N \times L}. \quad (5.15)$$

Note that  $\mathbf{C}$  only determines which states of the AS that is considered as an output by the DE. Thus it is a purely conceptual matrix with no physical implementation. With this choice of  $\mathbf{C}$ , only the last state of the AS is treated as an output. It is also possible to consider multiple outputs and this will indeed give increased performance. However, for simplicity, only the single output case is treated in this report.

For the multiple input case, i.e.  $L > 1$ , we define  $N = LN_\ell$ , where  $N_\ell$  is the order of the single input system. Due to the shape of the parametrization matrices, we restrict both  $N_\ell$  and  $L$  to be powers of 2. For  $L > 1$ , the state-space matrices generalizes as

$$\mathbf{L}_{N/2} = \begin{bmatrix} \mathbf{L}_{N_\ell/2} & & \\ & \ddots & \\ & & \mathbf{L}_{N_\ell/2} \end{bmatrix} \in \mathbb{R}^{\frac{N}{2} \times \frac{N}{2}}, \quad (5.16)$$

$$\mathbf{B}' = \begin{bmatrix} \mathbf{B}'_\ell & & \\ & \ddots & \\ & & \mathbf{B}'_\ell \end{bmatrix} \in \mathbb{R}^{N \times L} \quad (5.17)$$

and

$$\mathbf{C}' = \begin{bmatrix} \mathbf{C}'_\ell & & \\ & \ddots & \\ & & \mathbf{C}'_\ell \end{bmatrix} \in \mathbb{R}^{N \times L}. \quad (5.18)$$

With  $N = LN_\ell$  and  $\mathbf{L}_{N/2}$  as above,  $\mathbf{A}, \mathbf{B}$  and  $\mathbf{C}^\top$  is still given by (5.8)-(5.10). In this single output case, the transfer function is a column vector given by

$$\mathbf{G}(\omega) = \mathbf{C}^\top (j\omega \mathbf{I}_N - \mathbf{A})^{-1} \mathbf{B} \quad (5.19)$$

$$= \mathbf{C}^\top (j\omega \mathbf{I}_N - \mathbf{H}'_N \mathbf{A}')^{-1} \mathbf{H}'_N \mathbf{B}', \quad (5.20)$$



where each element gives the transfer function of the corresponding input. It is shown in appendix A that all inputs will have the same transfer function, given by

$$G(\omega) = \left( \sqrt{\frac{N}{2}} \frac{\beta}{j\omega} \right)^{N_\ell} \quad (5.21)$$

A hardware implementation of the proposed AS is shown in figure 5.2 for  $N = 8$  and  $L = 2$ . For this example,  $\mathbf{A}$  is given by

$$\begin{aligned} \mathbf{A} &= \mathbf{H}'_8 \mathbf{A}' \quad (5.22) \\ &= \begin{pmatrix} 1 & 1 & 1 & 1 & 0 & 0 & 0 & 0 \\ 1 & -1 & 1 & -1 & 0 & 0 & 0 & 0 \\ 1 & 1 & -1 & -1 & 0 & 0 & 0 & 0 \\ 1 & -1 & -1 & 1 & 0 & 0 & 0 & 0 \\ 0 & 0 & 0 & 0 & 1 & 1 & 1 & 1 \\ 0 & 0 & 0 & 0 & 1 & -1 & 1 & -1 \\ 0 & 0 & 0 & 0 & 1 & 1 & -1 & -1 \\ 0 & 0 & 0 & 0 & 1 & -1 & -1 & 1 \end{pmatrix} \begin{pmatrix} 0 & 0 & 0 & 0 & 0 & 0 & 0 & 0 \\ 0 & 0 & 0 & 0 & \beta & 0 & 0 & 0 \\ 0 & 0 & 0 & 0 & 0 & 0 & 0 & 0 \\ 0 & 0 & 0 & 0 & 0 & 0 & \beta & 0 \\ \beta & 0 & 0 & 0 & 0 & 0 & 0 & 0 \\ 0 & \beta & 0 & 0 & 0 & 0 & 0 & 0 \\ 0 & 0 & \beta & 0 & 0 & 0 & 0 & 0 \\ 0 & 0 & 0 & \beta & 0 & 0 & 0 & 0 \end{pmatrix}. \quad (5.23) \end{aligned}$$

The Hadamard matrices  $\mathbf{H}_4(Z)$  is easily implemented as shown in figure 5.1. The integrators can be implemented using either operational voltage- or transconductance amplifiers.

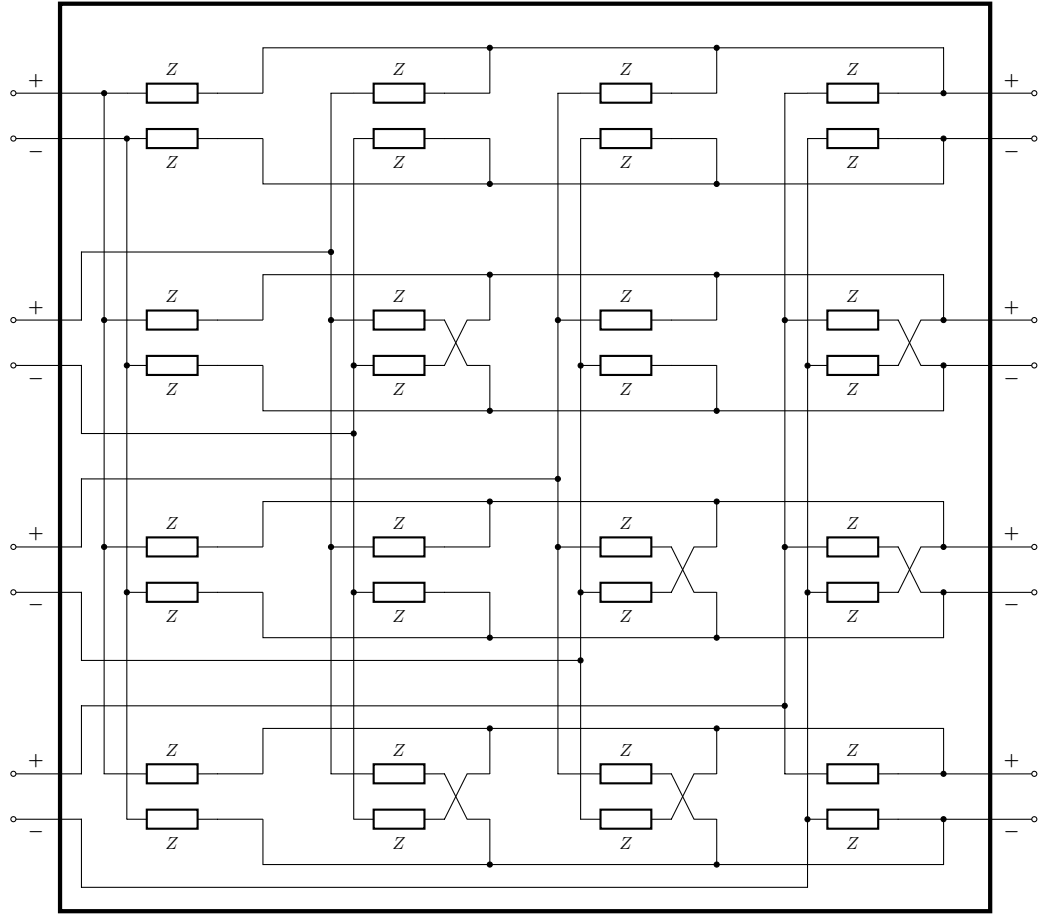


Figure 5.1: A 4th order Hadamard matrix implemented with impedance  $Z$ . Straight wires correspond to a multiplication of 1 and crossing wires to multiplication of  $-1$

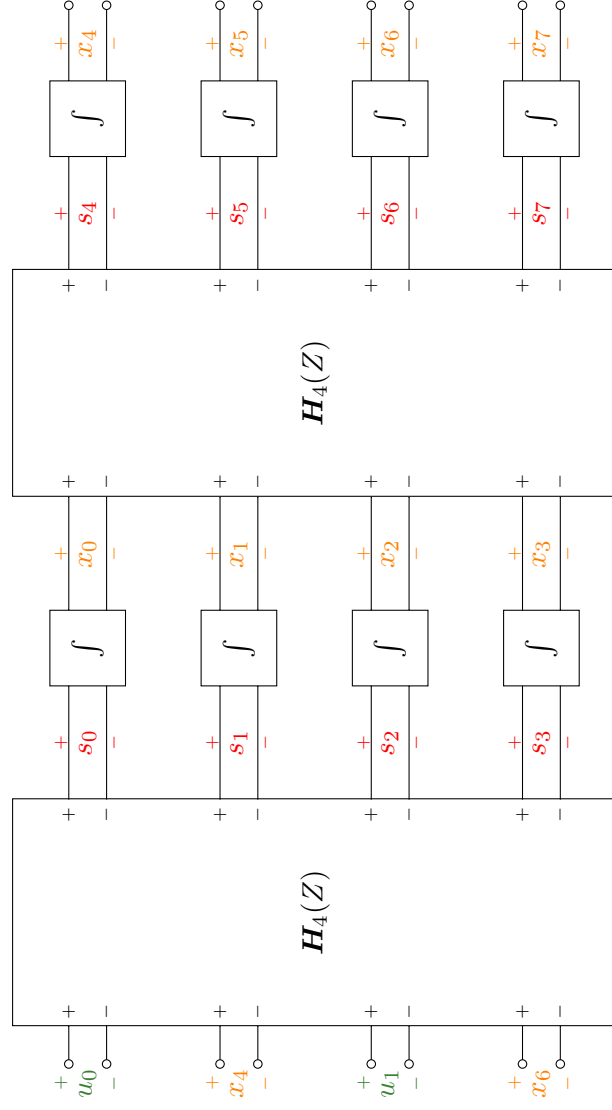
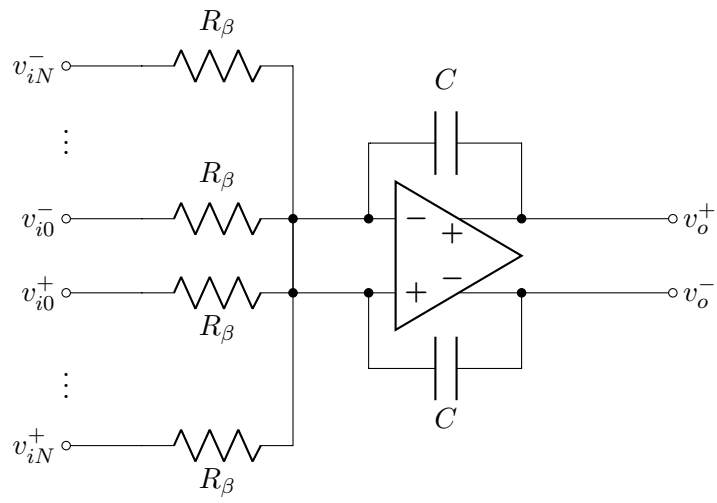
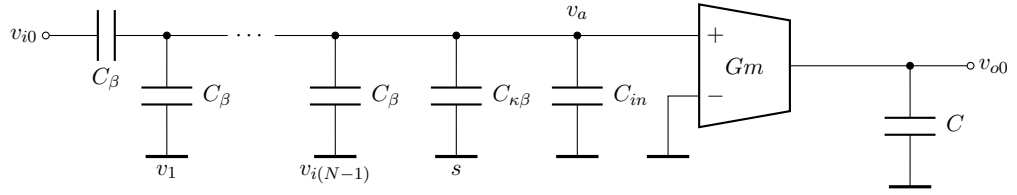
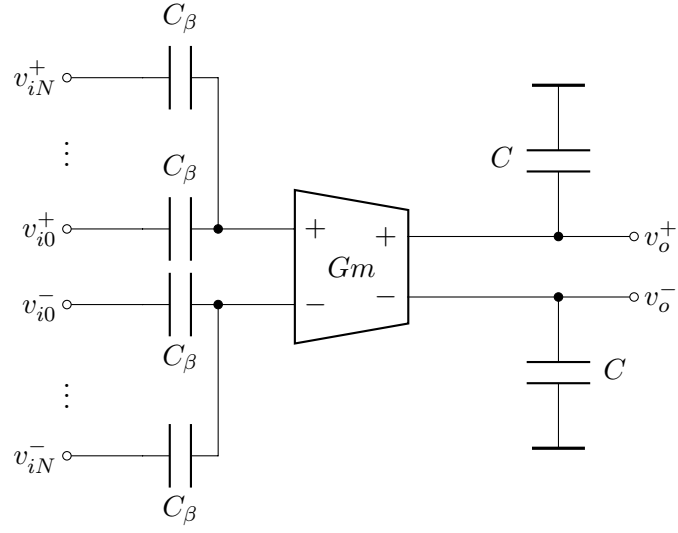


Figure 5.2: Proposed hardware implementation of the Hadamard ADC AS for  $N=8, L=2$



## Appendix A

# Transfer Function Analysis

This appendix contains the derivation of the transfer function of the AS described by equations 5.8, 5.9 and 5.10. It will become apparent that for multiple inputs, i.e.  $L > 1$ , the transfer function decouples into a set of identical expressions. For this analysis, we first consider the case of single input and then show how the obtained results generalizes for the multiple input case. For a single input, the transfer function is a scalar given by

$$G(\omega) = \mathbf{C}^\top (j\omega \mathbf{I}_N - \mathbf{A})^{-1} \mathbf{B} \quad (\text{A.1})$$

$$= \mathbf{C}^\top (j\omega \mathbf{I}_N - \mathbf{H}'_N \mathbf{A}')^{-1} \mathbf{H}'_N \mathbf{B}' \quad (\text{A.2})$$

$$= \mathbf{C}^\top \mathbf{M}^{-1} \mathbf{H}'_N \mathbf{B}', \quad (\text{A.3})$$

where we have defined  $\mathbf{M} \triangleq (j\omega \mathbf{I}_N - \mathbf{H}'_N \mathbf{A}') \in \mathbb{R}^{N \times N}$ . To obtain an analytic expression for the transfer function, we first need a closed form expression for the inverse of this matrix. Referring to equations 5.11 and 5.12, the matrix  $\mathbf{M}$  can be expressed in block form as

$$\mathbf{M} = \begin{bmatrix} \mathbf{M}_{11} & \mathbf{M}_{21} \\ \mathbf{M}_{12} & \mathbf{M}_{22} \end{bmatrix} = \begin{bmatrix} j\omega \mathbf{I}_{N/2} & -\beta \mathbf{H}_{N/2} \mathbf{L}_{N/2} \\ -\beta \mathbf{H}_{N/2} & j\omega \mathbf{I}_{N/2} \end{bmatrix}. \quad (\text{A.4})$$

The general inverse of a block matrix can be expressed using

$$\mathbf{D}_1 = \mathbf{M}_{11} - \mathbf{M}_{12} \mathbf{M}_{22}^{-1} \mathbf{M}_{21} \quad (\text{A.5})$$

and

$$\mathbf{D}_2 = \mathbf{M}_{22} - \mathbf{M}_{21} \mathbf{M}_{11}^{-1} \mathbf{M}_{12} \quad (\text{A.6})$$

as

$$\mathbf{M}^{-1} = \begin{bmatrix} \mathbf{D}_1^{-1} & -\mathbf{M}_{11}^{-1} \mathbf{M}_{12} \mathbf{D}_2^{-1} \\ -\mathbf{D}_2^{-1} \mathbf{M}_{21} \mathbf{M}_{11}^{-1} & \mathbf{D}_2^{-1} \end{bmatrix}. \quad (\text{A.7})$$

For this particular matrix,  $\mathbf{D}_1$  and  $\mathbf{D}_2$  coincide as

$$\mathbf{D} = j\omega \mathbf{I}_{N/2} - \frac{\beta^2}{j\omega} \frac{N}{2} \mathbf{L}_{N/2} \quad (\text{A.8})$$

and the inverse of  $\mathbf{M}$  can then be written as

$$\mathbf{M}^{-1} = \begin{bmatrix} \mathbf{D}^{-1} & \frac{\beta}{j\omega} \mathbf{H}_{N/2} \mathbf{L}_{N/2} \mathbf{D}^{-1} \\ \frac{\beta}{j\omega} \mathbf{D}^{-1} \mathbf{H}_{N/2} & \mathbf{D}^{-1} \end{bmatrix}. \quad (\text{A.9})$$

It remains to find an expression for  $\mathbf{D}^{-1}$ . We first define the parameter  $\psi \triangleq \frac{\beta^2}{(j\omega)^2} \frac{N}{2}$  and write

$$\mathbf{D} = j\omega (\mathbf{I}_{N/2} - \psi \mathbf{L}_{N/2}). \quad (\text{A.10})$$

By (5.13), the matrix  $\mathbf{L}_{N/2}$  is strictly lower triangular which implies that  $\mathbf{L}_{N/2}^k = \mathbf{0}$  for some  $k > 0$ . We can therefore express  $\mathbf{D}^{-1}$  by the Neumann series (generalized geometric series) of  $\mathbf{L}_{N/2}$  as

$$\mathbf{D}^{-1} = \frac{1}{j\omega} (\mathbf{I}_{N/2} - \psi \mathbf{L}_{N/2})^{-1} \quad (\text{A.11})$$

$$= \frac{1}{j\omega} \sum_{k=0}^{\infty} \psi^k \mathbf{L}_{N/2}^k \quad (\text{A.12})$$

$$= \frac{1}{j\omega} \left( \mathbf{I}_{N/2} + \sum_{k=1}^{\frac{N}{2}-1} \psi^k \mathbf{L}_{N/2}^k \right). \quad (\text{A.13})$$

Because of the shape of  $\mathbf{L}_{N/2}$ , the matrix  $\left( \mathbf{I}_{N/2} + \sum_{k=1}^{\frac{N}{2}-1} \psi^k \mathbf{L}_{N/2}^k \right)$  will have the form

$$\left( \mathbf{I}_{N/2} + \sum_{k=1}^{\frac{N}{2}-1} \psi^k \mathbf{L}_{N/2}^k \right) = \begin{pmatrix} 1 & 0 & & & \\ \psi & 1 & 0 & & \\ \psi^2 & \psi & 1 & 0 & \\ \vdots & \ddots & \ddots & \ddots & 0 \\ \psi^{\frac{N}{2}-1} & \dots & \psi^2 & \psi & 1 \end{pmatrix} \quad (\text{A.14})$$

To obtain a compact expression, we introduce the vector

$$\boldsymbol{\psi}_i^M \triangleq \begin{pmatrix} \mathbf{0}_i \\ \psi^0 \\ \psi \\ \vdots \\ \psi^{M-1-i} \end{pmatrix}, \quad (\text{A.15})$$

where  $\mathbf{0}_i \in \mathbb{R}^i$  is an all-zero column vector of length  $i$ . Using this vector, we write

$$\left( \mathbf{I}_{N/2} + \sum_{k=1}^{\frac{N}{2}-1} \psi^k \mathbf{L}_{N/2}^k \right) = \boldsymbol{\Psi}_{N/2} \quad (\text{A.16})$$

where

$$\Psi_{N/2} \triangleq \begin{bmatrix} \psi_0^{N/2} & \cdots & \psi_{N/2-1}^{N/2} \end{bmatrix}. \quad (\text{A.17})$$

After the introduction of this helper matrix, we can write the expression for the transfer function as

$$G(\omega) = \mathbf{C}^\top \begin{bmatrix} \mathbf{D}^{-1} & \frac{\beta}{j\omega} \mathbf{H}_{N/2} \mathbf{L}_{N/2} \mathbf{D}^{-1} \\ \frac{\beta}{j\omega} \mathbf{D}^{-1} \mathbf{H}_{N/2} & \mathbf{D}^{-1} \end{bmatrix} \mathbf{H}'_N \mathbf{B} \quad (\text{A.18})$$

$$= \mathbf{C}^\top \begin{bmatrix} \frac{1}{j\omega} \Psi_{N/2} & \frac{\beta}{(j\omega)^2} \mathbf{H}_{N/2} \mathbf{L}_{N/2} \Psi_{N/2} \\ \frac{\beta}{(j\omega)^2} \Psi_{N/2} \mathbf{H}_{N/2} & \frac{1}{j\omega} \Psi_{N/2} \end{bmatrix} \mathbf{H}'_N \mathbf{B} \quad (\text{A.19})$$

Before proceeding, we recognize the following. As

$$\mathbf{B}' = (\beta \quad 0 \quad \cdots \quad 0)^\top \in \mathbb{R}^{N \times 1} \quad (\text{A.20})$$

we get

$$\mathbf{H}'_N \mathbf{B}' = \beta \begin{bmatrix} \mathbf{1}_{N/2} \\ \mathbf{0}_{N/2} \end{bmatrix}. \quad (\text{A.21})$$

Together with  $\mathbf{C}^\top = (0 \quad \cdots \quad 1)$  we see that only  $(\mathbf{M}^{-1})_{11} = \frac{\beta}{(j\omega)^2} \Psi_{N/2} \mathbf{H}_{N/2}$  will influence the transfer function, and we can write

$$G(\omega) = (0 \quad \cdots \quad 1) \frac{\beta}{(j\omega)^2} \Psi_{N/2} \mathbf{H}_{N/2} \beta \mathbf{1}_{N/2} \quad (\text{A.22})$$

$$= \frac{\beta^2}{(j\omega)^2} (0 \quad \cdots \quad 1) \Psi_{N/2} \mathbf{H}_{N/2} \mathbf{1}_{N/2} \quad (\text{A.23})$$

The matrix product  $\Psi_{N/2} \mathbf{H}_{N/2} \mathbf{1}_{N/2}$  can be analyzed recursively as

$$\Psi_{N/2} \mathbf{H}_{N/2} \mathbf{1}_{N/2} = \begin{bmatrix} \Psi_{N/4} & \mathbf{0}_{N/4 \times N/4} \\ \hat{\Psi}_{N/4} & \Psi_{N/4} \end{bmatrix} \begin{bmatrix} \mathbf{H}_{N/4} & \mathbf{H}_{N/4} \\ \mathbf{H}_{N/4} & -\mathbf{H}_{N/4} \end{bmatrix} \mathbf{1}_{N/2} \quad (\text{A.24})$$

$$= 2 \begin{bmatrix} \Psi_{N/4} \mathbf{H}_{N/4} \mathbf{1}_{N/4} \\ \hat{\Psi}_{N/4} \mathbf{H}_{N/4} \mathbf{1}_{N/4} \end{bmatrix}, \quad (\text{A.25})$$

where

$$\hat{\Psi}_{N/4} \triangleq \begin{bmatrix} \psi^{N/4} \psi_0 & \cdots & \psi \psi_0 \end{bmatrix}. \quad (\text{A.26})$$

Furthermore,

$$\hat{\Psi}_{N/4} \mathbf{H}_{N/4} \mathbf{1}_{N/4} = \begin{bmatrix} \psi^{N/8} \hat{\Psi}_{N/8} & \hat{\Psi}_{N/8} \\ \psi^{N/4} \hat{\Psi}_{N/8} & \psi^{N/8} \hat{\Psi}_{N/8} \end{bmatrix} \begin{bmatrix} \mathbf{H}_{N/8} & \mathbf{H}_{N/8} \\ \mathbf{H}_{N/8} & -\mathbf{H}_{N/8} \end{bmatrix} \mathbf{1}_{N/2} \quad (\text{A.27})$$

$$= 2 \begin{bmatrix} \psi^{N/8} \hat{\Psi}_{N/8} \mathbf{H}_{N/8} \mathbf{1}_{N/8} \\ \psi^{N/4} \hat{\Psi}_{N/8} \mathbf{H}_{N/8} \mathbf{1}_{N/8} \end{bmatrix}. \quad (\text{A.28})$$

Starting at

$$\hat{\Psi}_1 \mathbf{H}_1 \mathbf{1}_1 = \psi, \quad (\text{A.29})$$

these recursive expressions may be combined to give

$$\mathbf{\Psi}_{N/2} \mathbf{H}_{N/2} \mathbf{1}_{N/2} = \frac{N}{2} \psi_0^{N/2}. \quad (\text{A.30})$$

Finally, the transfer function is given by

$$G(\omega) = (0 \ \cdots \ 1) \frac{\beta}{(j\omega)^2} \mathbf{\Psi}_{N/2} \mathbf{H}_{N/2} \beta \mathbf{1}_{N/2} \quad (\text{A.31})$$

$$= \frac{\beta^2}{(j\omega)^2} \frac{N}{2} (0 \ \cdots \ 1) \psi_0^{N/2} \quad (\text{A.32})$$

$$= \frac{\beta^2}{(j\omega)^2} \frac{N}{2} \psi^{N/2-1} \quad (\text{A.33})$$

$$= \left( \frac{\beta^2}{(j\omega)^2} \frac{N}{2} \right)^{N/2} \quad (\text{A.34})$$

$$= \left( \sqrt{\frac{N}{2}} \frac{\beta}{j\omega} \right)^N \quad (\text{A.35})$$

### Multiple inputs

The transfer function expression (A.35) was derived assuming a single input only. We now show how this results generalizes for multiple inputs. We consider the case of  $L = 2$  inputs and the extension to arbitrary  $L$  is straightforward.

For  $L > 1$ , we let  $N \triangleq N_\ell L$ , where  $N_\ell$  is the system order for a single channel. For  $L = 2$  we have

$$\mathbf{C}^\top = \begin{pmatrix} \mathbf{0}_{N/2}^\top & 0 & \cdots & 1 & 0 & \cdots & 0 \\ \mathbf{0}_{N/2}^\top & 0 & \cdots & 0 & 0 & \cdots & 1 \end{pmatrix} \in \mathbb{R}^{2 \times N}, \quad (\text{A.36})$$

$$\mathbf{B}' = \begin{pmatrix} \beta & \cdots & 0 & 0 & \cdots & 0 & \mathbf{0}_{N/2}^\top \\ 0 & \cdots & 0 & \beta & \cdots & 0 & \mathbf{0}_{N/2}^\top \end{pmatrix}^\top \in \mathbb{R}^{N \times 2}, \quad (\text{A.37})$$

and

$$\mathbf{H}'_N \mathbf{B}' = \beta \begin{bmatrix} \mathbf{1}_{N_\ell/2} & \mathbf{1}_{N_\ell/2} \\ \mathbf{1}_{N_\ell/2} & -\mathbf{1}_{N_\ell/2} \\ \mathbf{0}_{N/2} & \mathbf{0}_{N/2} \end{bmatrix} \in \mathbb{R}^{N \times 2}, \quad (\text{A.38})$$

$\mathbf{A}'$  is as given by (5.12), but with

$$\mathbf{L}_{N/2} \triangleq \begin{bmatrix} \mathbf{L}_{N_\ell/2} & \mathbf{0}_{N_\ell/2 \times N_\ell/2} \\ \mathbf{0}_{N_\ell/2 \times N_\ell/2} & \mathbf{L}_{N_\ell/2} \end{bmatrix}. \quad (\text{A.39})$$



In (A.12) we used the power series of  $\mathbf{L}_{N/2}$ . For  $L = 2$  we have

$$\mathbf{L}_{N/2}^k = \begin{bmatrix} \mathbf{L}_{N\ell/2} & \mathbf{0}_{N\ell/2 \times N\ell/2} \\ \mathbf{0}_{N\ell/2 \times N\ell/2} & \mathbf{L}_{N\ell/2} \end{bmatrix}^k \quad (\text{A.40})$$

$$= \begin{bmatrix} \mathbf{L}_{N\ell/2}^k & \mathbf{0}_{N\ell/2 \times N\ell/2} \\ \mathbf{0}_{N\ell/2 \times N\ell/2} & \mathbf{L}_{N\ell/2}^k \end{bmatrix}, \quad (\text{A.41})$$

and in consequence

$$\mathbf{\Psi}_{N/2} = \begin{bmatrix} \mathbf{\Psi}_{N\ell/2} & \mathbf{0}_{N\ell/2 \times N\ell/2} \\ \mathbf{0}_{N\ell/2 \times N\ell/2} & \mathbf{\Psi}_{N\ell/2} \end{bmatrix}. \quad (\text{A.42})$$

Furthermore

$$\mathbf{\Psi}_{N/2} \mathbf{H}_{N/2} = \begin{bmatrix} \mathbf{\Psi}_{N\ell/2} & \mathbf{0}_{N\ell/2 \times N\ell/2} \\ \mathbf{0}_{N\ell/2 \times N\ell/2} & \mathbf{\Psi}_{N\ell/2} \end{bmatrix} \begin{bmatrix} \mathbf{H}_{N\ell/2} & \mathbf{H}_{N\ell/2} \\ \mathbf{H}_{N\ell/2} & -\mathbf{H}_{N\ell/2} \end{bmatrix} \quad (\text{A.43})$$

$$= \begin{bmatrix} \mathbf{\Psi}_{N\ell/2} \mathbf{H}_{N\ell/2} & \mathbf{\Psi}_{N\ell/2} \mathbf{H}_{N\ell/2} \\ \mathbf{\Psi}_{N\ell/2} \mathbf{H}_{N\ell/2} & -\mathbf{\Psi}_{N\ell/2} \mathbf{H}_{N\ell/2} \end{bmatrix}, \quad (\text{A.44})$$

and

$$\mathbf{\Psi}_{N/2} \mathbf{H}_{N/2} \begin{bmatrix} \mathbf{1}_{N\ell/2} & \mathbf{1}_{N\ell/2} \\ \mathbf{1}_{N\ell/2} & -\mathbf{1}_{N\ell/2} \end{bmatrix} = \begin{bmatrix} 2\mathbf{\Psi}_{N\ell/2} \mathbf{H}_{N\ell/2} & \mathbf{0}_{N\ell/2} \\ \mathbf{0}_{N\ell/2} & 2\mathbf{\Psi}_{N\ell/2} \mathbf{H}_{N\ell/2} \end{bmatrix}, \quad (\text{A.45})$$

The expression for the transfer function then becomes

$$\mathbf{G}(\omega) = \frac{\beta^2}{(j\omega)^2} \begin{pmatrix} 0 & \cdots & 1 & 0 & \cdots & 0 \\ 0 & \cdots & 0 & 0 & \cdots & 1 \end{pmatrix} \mathbf{\Psi}_{N/2} \mathbf{H}_{N/2} \begin{bmatrix} \mathbf{1}_{N\ell/2} & \mathbf{1}_{N\ell/2} \\ \mathbf{1}_{N\ell/2} & -\mathbf{1}_{N\ell/2} \end{bmatrix} \quad (\text{A.46})$$

$$= \frac{2\beta^2}{(j\omega)^2} \begin{pmatrix} 0 & \cdots & 1 & 0 & \cdots & 0 \\ 0 & \cdots & 0 & 0 & \cdots & 1 \end{pmatrix} \begin{bmatrix} \mathbf{\Psi}_{N\ell/2} \mathbf{H}_{N\ell/2} & \mathbf{0}_{N\ell/2} \\ \mathbf{0}_{N\ell/2} & \mathbf{\Psi}_{N\ell/2} \mathbf{H}_{N\ell/2} \end{bmatrix} \quad (\text{A.47})$$

$$= \begin{pmatrix} \left( \sqrt{\frac{2N_\ell}{2}} \frac{\beta}{j\omega} \right)^{N_\ell} \\ \left( \sqrt{\frac{2N_\ell}{2}} \frac{\beta}{j\omega} \right)^{N_\ell} \end{pmatrix} = \begin{pmatrix} \left( \sqrt{\frac{N}{2}} \frac{\beta}{j\omega} \right)^{N_\ell} \\ \left( \sqrt{\frac{N}{2}} \frac{\beta}{j\omega} \right)^{N_\ell} \end{pmatrix}. \quad (\text{A.48})$$

From this derivation we see that for an ADC with an arbitrary number of input channels, the transfer function is

$$\mathbf{G}(\omega) = \left( \sqrt{\frac{N}{2}} \frac{\beta}{j\omega} \right)^{N_\ell} \quad (\text{A.49})$$

for all channels.

# Bibliography

- [1] T. C. Carusone, D. Johns, and K. Martin, *Analog Integrated Circuit Design, second edition*. John Wiley and Sons Inc., 2013.
- [2] H. Loeliger, L. Bolliger, G. Wilckens, and J. Biveroni, “Analog-to-digital conversion using unstable filters,” in *2011 Information Theory and Applications Workshop*, pp. 1–4, 2011.
- [3] H. Loeliger and G. Wilckens, “Control-based analog-to-digital conversion without sampling and quantization,” in *2015 Information Theory and Applications Workshop (ITA)*, pp. 119–122, 2015.
- [4] H.-A. Loeliger, H. Malmberg, and G. Wilckens, “Control-bounded analog-to-digital conversion: Transfer function analysis, proof of concept, and digital filter implementation,” 2020.
- [5] H. Malmberg, “Control-bounded converters.” 2020.
- [6] B. D. O. Anderson and J. B. Moore, *Optimal Filtering*. Prentice Hall, 1979.